High Efficiency Fiber-Chip Coupling

CNF Project Number: 2524-17
Principal Investigator(s): Jaime Cardenas
User(s): Sushant Kumar

Affiliation(s): The Institute of Optics, University of Rochester

Primary Source(s) of Research Funding: National Science Foundation - PFI

Contact: jaime.cardenas@rochester.edu, skumar31@ur.rochester.edu

Research Group Website: https://www.hajim.rochester.edu/optics/cardenas/

Primary CNF Tools Used: JEOL9500, ASML PAS 5500/300C DUV Stepper, Oxford PECVD, LPCVD Furnace, Oxford 100 Etcher, Unaxis 770 Deep Silicon Etcher, Plasma-Therm Versaline Silicon Etcher, Xactix Xenon Difluoride Etcher

Abstract:

We design and fabricate silicon photonic chips for high efficiency Polarization Maintaining optical fiber-chip coupling.

Summary of Research:

The need for increasingly large amounts of data and bandwidths has been driving the growth of Silicon Photonics for telecom and data-center applications. But this has also let to an increasing share of power consumption in the optical data-networks leading to development of more energy efficient designs like co-packaged optics [1], ring-based modulators [2], etc. These designs while being energy efficient are very sensitive to polarization. To ensure clean polarization devices can integrate laser sources on chip [3], which increases heat density on chip and introduces associated thermal instability and cross coupling issues that require more expensive cooling and careful design. More modern system designs [4] include external laser sources to reduce the heat density on chip but require PM fiber connections to the chip. To our knowledge there are no good industry level solutions for PM fiber connections.

Most widespread packaging solutions for PM fibers rely on micro lens assemblies and some recent work on angle thin polished PM fiber connection uses on chip gratings and epoxy [5], which makes the connection limited in bandwidth and heavily temperature dependent due the use of epoxy. In this project we designed high efficiency couplers for PM-fiber-chip coupling and measured to verify any depolarization effects caused by the connection itself.

We designed the SiO2 Mode Converter (MC) by matching the optical mode at the MC-fiber interface. This is done by optimizing the dimensions for the MC at the interface. This allows not only for efficient coupling of optical power due to minimized mode matching, but also increases the alignment tolerance of the fiber-chip connection by making the mode 10 μm in diameter as compared to regular waveguide tapers which have 3-4 μm diameter optical modes. On the other end of the MC, the dimensions of the MC and waveguide taper are optimized to maximize the power transfer. Since at this interface everything is lithographically designed, misalignment is not a concern and only the power coupling efficiency is of import. The input and output ports are offset laterally to eliminate any scattered light polluting the measurements.

We start with 5.75 μm of OXFORD-PECVD SiO2 on a blank Si wafer and then use a 300 nm thick OXFORD-PECVD deposited Si3N4 layer for waveguide layer. The waveguides are defined using the ASML-PAS-500 stepper and etched using the OXFORD-100 ICP-RIE. We deposit 5.75 μm SiO2 via OXFORD-PECVD and then pattern the SiO2 (MC) using the ASML PAS-5000. The SiO2 is etched using the OXFORD-100. Fiber grooves are etched into the chip using either UNAXIS 770 or the Plasma-Therm Versaline Deep Silicon Etcher. Once the grooves are etched the chips are undercut using the Xactix Xenon Difluoride Etcher to optically isolate the mode while it propagates in the SiO2 mode converter. The wafer is diced into chips using the DISCO dicing saw. Further details on the design and fabrication of devices can be found in the published paper [6].

For testing the coupling efficiency and the polarization extinction ratio (PER), light coming out of the PM fiber is used as baseline and the fiber is aligned to TE orientation using a free-space linear polarizer. Then the light is launched onto the chip and collected at the output using a high NA microscope objective to estimate the propagation loss of the chip. At this point the pre-fusion PER is also estimated and largely matches the

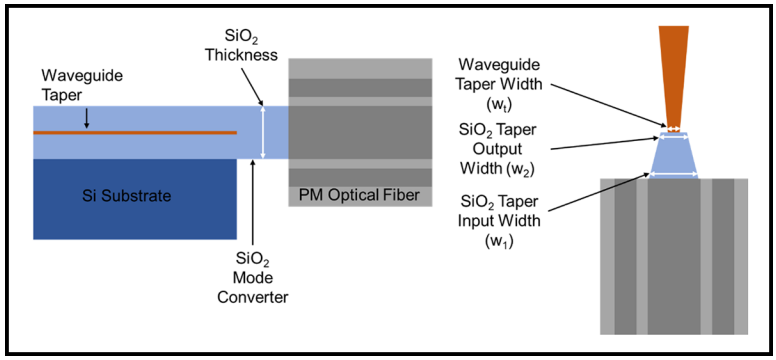

Figure 1: Chip design and material configuration.

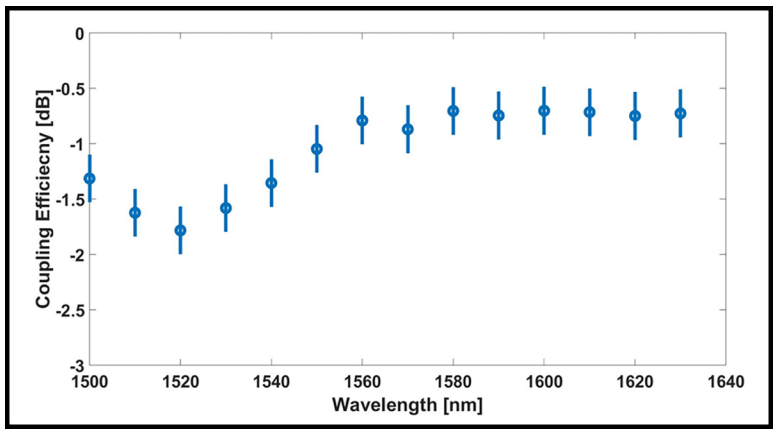

Figure 2: Coupling data for fused fiber-chip connection.

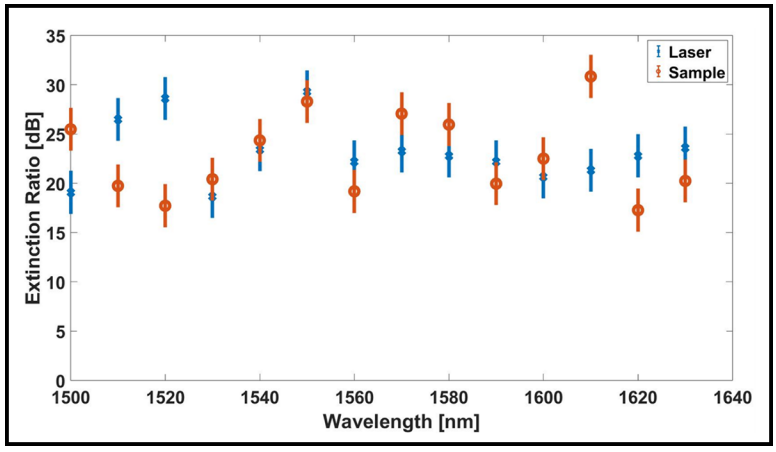

Figure 3: PER data for post-fusion PM-fiber-chip connection.

baseline stablished from the PM fiber. This indicates that the light coming out of the PM fiber doesn't depolarize as it couples to and travels through the chip. Then the objective is replaced with another optical fiber to estimate a pre-fusion coupling efficiency of 1.2dB. Then the fiber is fused to the chip using a CO2 laser and the light is again collected using the optical fiber at the other end and the post fusion coupling is estimated to be 1dB per facet. Then the fiber at the output is replaced with the high NA objective with a liner polarizer in the optical path, to again estimate the PER. As shown in Figure 2.

The PER post fusion also largely follows the baseline established from the PM fiber light leading to the conclusion that the fusion doesn't lead to any damage to the PM fiber structure or any depolarization of the light.

Conclusions and Future Steps:

In conclusion, we demonstrate efficient fiber to chip connection via CO2 laser fusion and show no degradation in polarization of the light that is being couple onto the chip. This demonstrates that the MC design and the laser fusion process are a viable option not only for standard single mode fibers-chip coupling but also for PM fibers. Further design, fabrication and testing is underway for other fiber configurations.

References:

[1] John Williamson, "Co-packaged optics, putting the pieces together," OpticalInterconnectNews.com, Issue 30, pp 20-21.

[2] M. Kim, M. Kim, Y. Jo, H. Kim, S. Lischke, C. Mai, L. Zimmermann, and W. Choi, "A Fully Integrated 25 Gb/s Si Ring Modulator Transmitter with a Temperature Controller," in Optical Fiber Communication Conference (OFC) 2020, OSA Technical Digest (Optica Publishing Group, 2020), paper T3H.7.

[3] P. J. Winzer, "Optical Networking Beyond WDM," in IEEE Photonics Journal, vol. 4, no. 2, pp. 647-651, April 2012, doi: 10.1109/JPHOT.2012.2189379.

[4] W. Zhou, Y. Zhu, J. Wang, M. Moewe, R. Zhu, W. Zhao, V. Rossin, H. Liu, J. Wang, T. Zhu, P. Yalamanchili, T. Pham, R. Chen, V. Zeng, and J. Stewart, "High Power CW Laser for Co-Packaged Optics," in Conference on Lasers and Electro-Optics, Technical Digest Series (Optica Publishing Group, 2022), paper SS2D.3.

[5] B. Snyder and P. O'Brien, "Packaging Process for Grating-Coupled Silicon Photonic Waveguides Using Angle-Polished Fibers," in IEEE Transactions on Components, Packaging and Manufacturing Technology, vol. 3, no. 6, pp. 954-959, June 2013, doi: 10.1109/TCPMT.2012.2237052.

[6] J. Nauriyal, M. Song, R. Yu, and J. Cardenas, "Fiber-to-chip fusion splicing for low-loss photonic packaging," Optica 6, 549-552 (2019).

Programmable Poling for Electric Field Induced Second Harmonic Generation

CNF Project Number: 2971-21
Principal Investigator(s): Peter McMahon[1,2]
User(s): Ryotatsu Yanagimoto[1,3], Benjamin Ash[1,3]

Affiliation(s): [1] School of Applied and Engineering Physics, Cornell University; [2] Kavli Institute at Cornell for Nanoscale Science, Cornell University; [3] NTT Physics and Informatics Laboratories, NTT Research, Inc.

Primary Source(s) of Research Funding: NSF Award CCF-1918549, David and Lucile Packard Foundation Fellowship, NTT Research, Air Force Office of Scientific Research Award Number FA9550-22-1-0378

Contact: pmcmahon@cornell.edu, ry338@cornell.edu baa77@cornell.edu

Primary CNF Tools Used: Oxford 100 PECVD, Even-Hour Evaporator, Woollam RC2 Spectroscopic Ellipsometer, Lesker PVD75 Sputter

Abstract:

Programmable photonics plays a vital role in modern technologies because of its low power consumption, high spatially parallelism, and high bandwidth. For most traditional devices, features are etched onto the device during fabrication, defining the device's utility. Recent device improvements enable programmability over a high number of spatial features, allowing a device to move beyond the one device, one function paradigm. Using this device, we demonstrated optical computation with spatially programmable index of refraction, but the same approach underlying this device can be extended into the nonlinear regime by performing electric-field induced second harmonic (E-Fish) generation. This work demonstrates proof-of-concept material development for a nonlinear lithography-free waveguide that converts 1550 nm light into 780 nm light with the ability to shape the wavefront of the generated signal. In the long term, this nonlinear programmability could enable light generation at nontraditional frequencies and spatially parallel computation.

Summary of Research:

Lithography-free photonics has attracted considerable attention in the field of programmable photonics because the large number of programmable parameters allows the device to move beyond the one device, one function paradigm. This means lithography-free devices can perform a large range of tasks and compensate for fabrication error [1]. Recent advances in lithography-free technology have enabled a device with real index of refraction modulation on-chip. In this device, a photoconductor and waveguiding layer with high native χ^2 nonlinearity are stacked in series and placed under high voltage, allowing the two layers act as a voltage divider. Because the index of refraction of the waveguiding layer depends on the electric bias, the index of refraction can be spatially controlled by shining different patterns of light onto the photoconductor [2]. Using the same device concept, the core material can be replaced with a material that displays large induced χ^2 during an electric-field induced second harmonic (E-Fish) process. Silicon nitride has previously demonstrated large induced χ^2 under a large electric bias, and our work successfully reproduced these results [3]. Furthermore, devices fabricated in the CNF displayed programmable E-Fish, showing that we can program the poling period and measure the increased second harmonic signal at the output. Finally, potential doped oxynitride claddings have been fabricated on the PECVD system which have the potential to make a more efficient, continuous-operation device.

Silicon-Rich Silicon Nitride Development. Using a PECVD system, we deposit silicon nitride films with low optical loss over a wide range of visible and infrared wavelengths. By adjusting the silane flow during deposition, we can tune the index of refraction from 1.9 to 2.4 at a wavelength of 1 μm. Moreover, these films display high photoconductivity, with a 100X conductivity switching ratio when pumped with a 532 nm laser. To characterize the film's induced χ^2, we deposit our SiNx films onto conductive Si substrates with 1.4 μm of thermal oxide. After sputtering ITO onto the SiNx layer, we pump the sample with 1535 nm light and record the power of 776 nm light generated as a function of applied DC voltage. By comparing this signal to the signal generated by LiNbO3 (which has a well-characterized native χ^2), we can estimate the effective χ^2 in our films as we increase the applied electric field.

Figure 1 shows the measured χ^2 for our silicon nitride and other similar films, which are consistent with

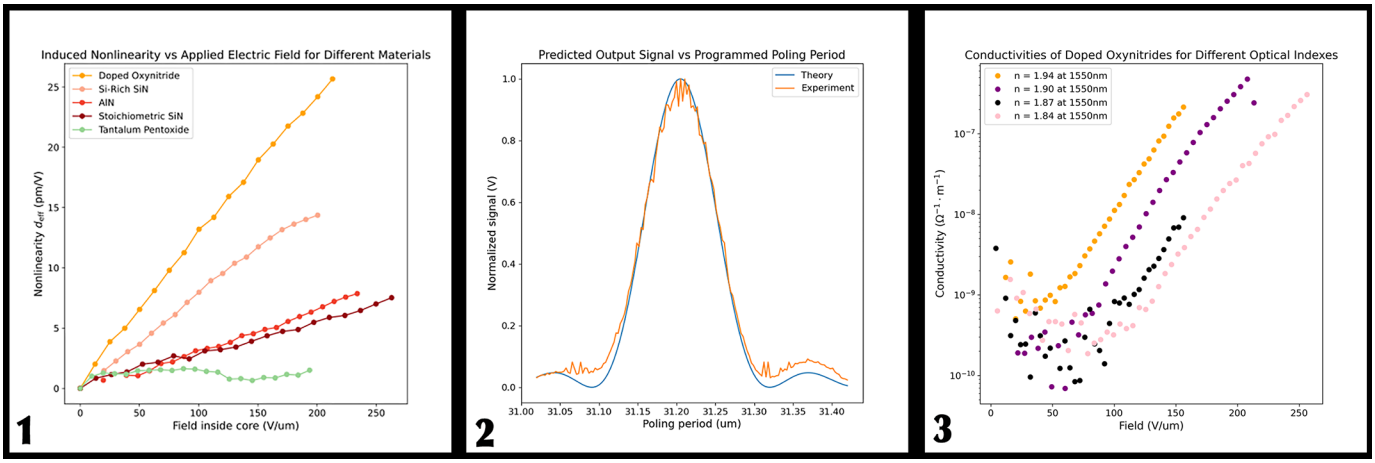

Figure 1: Silicon-rich nitride shows exceptionally high induced nonlinearity under large applied electric fields. When compared to other materials, silicon-rich silicon nitride has high induced nonlinearity. Its high optical index and low optical loss over a wide range of visible and infrared frequencies make it a desirable core material for a programmable nonlinear device.

Figure 2: Comparison of the predicted generated output power versus the experimental output power for different applied poling periods. The close agreement between experiment and theory proves that we can program the poling period to satisfy the phase matching condition for E-Fish. This procedure can be executed for different wavelengths and waveguide dispersions.

Figure 3: Characterization of the electric conductivity of boron-doped silicon oxynitrides. Doped oxynitrides display exceptionally high conductivities given their low optical indexes. Moreover, these conductivity curves show that both index and conductivity can be tuned by adjusting the N2O or B2H6 flow. These characteristics, combined with losses below 5 dB/cm across a broad range of infrared frequencies, make these films ideal claddings for a continuous operation device.

recent measurements on similar materials [3]. When these films are integrated into a programmable device, we can apply different poling periods to satisfy the phase-matching condition for E-Fish. Our device design consisted of SiNx waveguide cores with SiO2 claddings. By applying a low-AC bias to the film, we could optimize the impedance of each film to achieve the highest field contrast between SiNx in the bright and dark state. Figure 2 demonstrates a device where we apply varying poling periods and optimize this period to achieve the largest output signal.

Doped Oxynitride Development. In our current device configuration, there is an impedance mismatch between the cladding and core layers of the device at DC. This means the higher impedance layers (specifically the oxides) will dominate the impedance of the stack at DC and reduce the switching ratio. While we can apply AC voltage to correct for this issue, this causes our devices to have lower modulation efficiencies and to operate non-continuously. One solution to this problem is fabricating low-loss, low-index, conductive cladding materials where we can change the deposition parameters to tune the index and conductivity. Films have already been demonstrated to achieve these types of parameters using boron-doped silicon oxynitrides, so we modified these recipes to integrate them into our devices [4]. Figure 3 shows the characterized conductivities of these films, which are repeatable across different depositions. In the future, we hope to integrate our SiNx and doped oxynitride films to make a continuous operation nonlinear programmable waveguide which can perform E-Fish generation and optical parametric amplification to generate different frequencies.

Acknowledgements:

The authors wish to thank National Science Foundation funding (award CCF-1918549). PLM gratefully acknowledges financial support from a David and Lucile Packard Foundation Fellowship. The authors wish to thank NTT Research for their financial and technical support. We gratefully acknowledge the Air Force Office of Scientific Research for funding under Award Number FA9550-22-1-0378. This work was performed in part at the Cornell NanoScale Facility, a member of the NNCI, which is supported by NSF Grant NNCI-2025233.

References:

[1] P. L. McMahon, Nature Reviews Physics 5, 717 (2023).

[2] T. Onodera, et al, Scaling on-chip photonic neural processors using arbitrarily programmable wave propagation (2024), arXiv:2402.17750.

[3] E. Timurdogan, C. V. Poulton, M. J. Byrd, and M. R.Watts, Nature Photonics 11, 200 (2017).

[4] N. Brinkmann, D. Sommer, G. Micard, G. Hahn, and B. Terheiden, Solar Energy Materials and Solar Cells 108, 180 (2013), selected publications from the 22nd Space Photovoltaic Research and Technology (SPRAT) Conference.

HfO_2-Based Platform for High Index Contrast Visible and UV Integrated Photonics

CNF Project Number: 2985-21
Principal Investigator(s): Karan Kartik Mehta[2]
User(s): Oscar Jaramillo[1,2]

Affiliation(s): 1. Applied and Engineering Physics, 2. Electrical and Computer Engineering; Cornell University

Primary Source(s) of Research Funding: NSF, Corning

Contact: karanmehta@cornell.edu, oj43@cornell.edu

Primary CNF Tools Used: Metricon, Zeiss Ultra SEM, JEOL 9500, PT770 Etcher, Woollam RC2 Spectroscopic Ellipsometer, AFM, Furnaces, Oxford PECVD, Keyence VHX-7100 Digital Microscope, Oxford FlexAL

Abstract:

We investigate photonic devices fabricated within a HfO_2/Al_2O_3 platform for high-index visible/ultraviolet photonics. Our findings show bulk optical losses of 2.8 ± 1.4 dB/cm and single-mode (SM) waveguide losses of 7.9 ± 1.7 dB/cm at a wavelength (λ) of 375 nm. At λ = 405 nm, SM waveguides show 2.6 ± 0.45 dB/cm. For λ = 730 nm, we measure a loaded quality factor (Q) of 1,840,000 bounding (SM) waveguide losses to <0.4 dB/cm. These results highlight the potential of $(HfO_2)_x/(Al_2O_3)_{1-x}$ devices and systems for visible and ultraviolet photonics.

Summary of Research:

Photonic integration at visible and UV wavelengths has applications in trapped-ion systems, spectroscopy, and other fields [1-3]. However, most common material platforms for integrated photonics absorb strongly in the UV, and increased surface and sidewall scattering at shorter wavelengths (scaling roughly as ~ λ^{-4}) pose a challenge in achieving low-loss waveguide structures. Silicon nitride (SiN) is a well-developed material with a high refractive index (~ 2.06 at λ = 405 nm), but experiences bulk optical losses of approximately 2.5 dB/cm at λ = 461 nm [4] and higher at shorter wavelengths [5]. Another material, aluminum oxide (Al_2O_3), has been used to demonstrate propagation losses of ~1.35 dB/cm at 369 nm [6,7], but suffers from a relatively low refractive index (~1.68 at λ = 405 nm). Hafnium dioxide (HfO_2), a CMOS compatible material, offers a high refractive index (~2.1 at λ = 405) and a wide band-gap

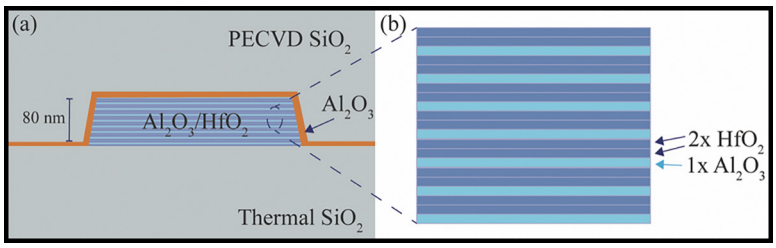

Figure 1: Waveguide cross-section showing an HfO_2-based core, a 4 nm thick Al_2O_3 diffusion barrier and PECVD SiO_2 cladding.

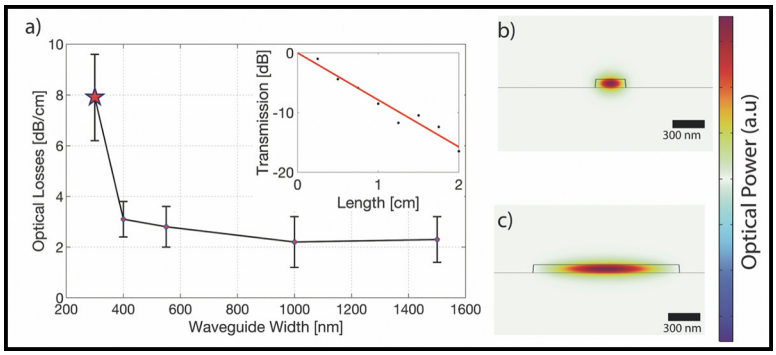

Figure 2: Optical micrograph of a representative device used to measure optical losses. To the right, an SEM image of a grating coupler used to couple light into the device.

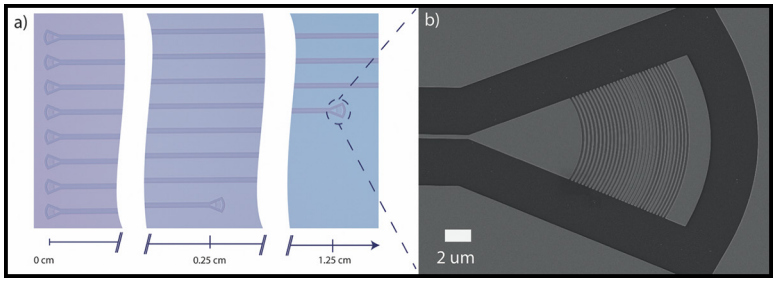

Figure 3: Measured optical losses for varying widths at 375 nm. Inset shows data obtained for a width of 300 nm.

material (5.65 eV) [8], but its tendency to crystallize limits its use in photonics to interaction lengths of ~ 100 nm [9,10]. Here we fabricate fully-cladded single mode (SM) and multimode (MM) waveguides using a low loss and high index HfO_2-based composite (~1.97 at $\lambda = 405$), composed of alternating layers of HfO_2 and Al_2O_3 deposited via Atomic Layer Deposition (ALD) [11,12]. We demonstrate an optical loss at $\lambda = 375$ nm of 7.9 ± 1.7 dB/cm for SM waveguides and measure bulk optical loss associate to bulk material loss to be 2.8 ± 1.4 dB/ cm at $\lambda = 375$ nm, and bound losses < 0.4 dB/cm at 730 nm from resonator measurements, indicating potential for this single high-index platform to span devices from the near UV to visible range.

Our platform consists of an 80nm-thick composite material deposited via ALD on a silicon wafer with 3 μm of thermally grown wet silicon oxide (Figure 1a). The composite material consists of single atomic layers of HfO_2 and Al_2O_3 with a duty cycle (DC) of 1/3 and a period (P) of 3, deposited via ALD at 300°C (Figure 1b). The characterization and choice of specific P and DC are discussed elsewhere [11,12]. After ALD deposition, we dice the wafer into pieces and anneal them at 800°C in a nitrogen environment for one hour. Each chip is processed separately by defining a pattern with electron beam lithography (JEOL9500) using ZEP520-A resist and etching with an inductively coupled plasma (ICP) etch using a BCl_3/Ar chemistry. The samples are then cleaned with a standard RCA clean. We deposit a ~ 4 nm layer of Al_2O_3 as a diffusion barrier and anneal again at 800°C for one hour. Finally, we deposit ~ 800 nm of plasma enhanced chemical vapor deposition (PECVD) SiO_2 as cladding.

We design and fabricate grating couplers to measure optical losses through a cutback configuration. Figure 2 shows subsections of a 4 cm long chip with input couplers and two output couplers at 0.25 cm and 1.25 cm, used to couple light in and out of the device from single-mode fibers. Figure 2b shows an SEM image of a representative grating for $\lambda = 405$ nm. We vary the width of the waveguide and measure the optical losses of each structure in order to discern sidewall scattering and bulk absorption. Figure 3a shows the measured optical loss as a function of width, with the inset showing a measurement obtained for a waveguide width of 300nm (indicated with a star on the plot). With increasing width, optical loss associated with sidewall scattering decreases and becomes dominated by bulk material loss. Quasi-TE optical modes measured for widths of 300 nm and 1500 nm are shown in Figure 3b and 3c, respectively.

A linear regression analysis [4] enables us to differentiate the fraction of optical loss arising from surface scattering vs. bulk loss. We find material loss to be 2.8 ± 1.4 dB/cm at $\lambda = 375$ nm.

Conclusions and Future Steps:

This work demonstrates that HfO_2 can be used to obtain competitive optical loss at $\lambda = 375$ and a higher refractive index than Al_2O_3. We observe that optical loss is dominated by sidewall scattering, indicating that fabrication optimization can enable even lower optical losses in SM waveguides. This work may lead to significantly more efficient grating devices, compact footprints, and micro-resonant structures, among others, for photonics at blue/UV wavelengths as compared to platforms in pure Al_2O_3 or SiN. Future work will determine the ultimate loss at shorter wavelengths.

References:

[1] D.J. Blumenthal. Photonic integration for UV to IR applications. APL Photonics 5, 020903, 2020.

[2] G. Moody, et al. Roadmap on integrated quantum photonics. J. Phys. Photonics 4 012501. 2022.

[3] Mehta, K., et al. Integrated optical addressing of an ion qubit. Nature Nanotech 11,1066-1070, 2016.

[4] M. Corato-Zanarella, et al, "Absorption and scattering limits of silicon nitride integrated photonics in the visible spectrum," Opt. Express 32, 5718-5728 (2024).

[5] C. Sorace-Agaskar, et al., "Versatile Silicon Nitride and Alumina Integrated Photonic Platforms for the Ultraviolet to Short-Wave Infrared," in IEEE Journal of Selected Topics in Quantum Electronics, vol. 25, no. 5, pp. 1-15, Sept. Oct. 2019, Art no. 8201515, doi: 10.1109/JSTQE.2019.2904443.

[6] Kwon, J., et al. Multi-site integrated optical addressing of trapped ions. Nat Commun 15, 3709 (2024). https://doi.org/10.1038/s41467-024-47882-5

[7] G.N. West, et al. Low-loss integrated photonics for the blue and ultraviolet regime. APL Photonics 4, 026101, 2019.

[8] L. Kang, B. H. Lee,W.-J. Qi, Y. Jeon, R. Nieh, S. Gopalan, K. Onishi, and J. C. Lee. Electrical characteristics of highly reliable ultrathin hafnium oxide gate dielectric. IEEE Electron Device Letters, vol. 21, no. 4, pp. 181-183, 2000.

[9] P. Torchio, A. Gatto, M. Alvisi, G. Albrand, N. Kaiser, and C. Amra. High-reflectivity HfO_2/SiO_2 ultraviolet mirrors. Applied Optics, vol. 41, no. 16, pp. 3256-3261, 2002.

[10] Zhang, C., et al. Low-loss metasurface optics down to the deep ultraviolet region. Light Sci Appl 9, 55, 2020.

[11] O. Jaramillo, L. Massai, and K. Mehta, "HfO2-based Platform for High Index Contrast Visible and UV Integrated Photonics," in CLEO 2023, Technical Digest Series (Optica Publishing Group, 2023), paper STh1O.6.

[12] Leonardo Massai. High Polarization Purity and Short-wavelength Optics for Trapped-ion Quantum Systems. Master's thesis, ETH, 2021.

Metamaterial Spectrometer: A Low SWaP, Robust, High Performance Hyperspectral Sensor for Land and Atmospheric Remote Sensing

CNF Project Number: 3003-22
Principal Investigator & User: Lori Lepak

Affiliation(s): Phoebus Optoelectronics LLC

Primary Source(s) of Research Funding: National Aeronautics and Space Administration (NASA)

Contact: llepak@phoebusopto.com

Research Group Website: www.phoebusopto.com

Primary CNF Tools Used: ASML DUV Stepper, Oxford ALD, Oxford PECVD, Ultra and Supra SEM, CHA Evaporator, Oxford 81 Etcher, Logitech CMP

Abstract:

Since 2003, Phoebus Optoelectronics has enabled custom R&D solutions in the fields of Plasmonics, Metamaterials, Antennas, and Sensors. We work closely with our customers throughout device development, from simulation and design, to prototype realization, testing, and small volume manufacturing. Our R&D portfolio spans the spectral ranges of visible light, infrared, terahertz (THz), and microwave radiation, for applications in high resolution imaging systems, wavelength and polarization filtering, tunable optical components, beam forming and steering, solar cells, renewable energy devices, and chemical and biological toxin sensors. We routinely partner with large, industry-leading businesses to develop products in all of these areas, jointly performing advanced testing and working together to scale up to medium- and large-volume manufacturing. Our agile team makes extensive use of the resources at the CNF for our nano/micro fabrication and testing, to provide cost efficiency and rapid turnaround.

In the present report, we discuss the ongoing development of a metamaterial-based hyperspectral imaging filter.

Summary of Research:

Phoebus uses the resources of the CNF to fabricate plasmonic chips patterned with a metamaterial surface to enable Extraordinary Optical Transmission (EOT), a phenomenon unique to metastructures in which light is transmitted through apertures much smaller than the incident wavelength, at anomalously large intensities relative to the predictions of conventional aperture theory. EOT was first observed by T.W. Ebbesen in 1998 [1]. Since its founding in 2003, Phoebus has successfully harnessed EOT by incorporating metasurfaces into devices used to perform light filtering [2-3], photon sorting [4-5], polarimetric detection [6], high speed optical detection [7], and SPR plasmonic sensor chips [8].

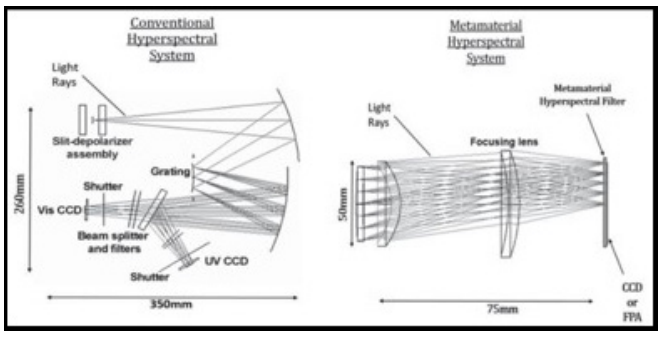

Figure 1: Phoebus's Metamaterial Spectrometer (MS) technology (right) eliminates much of the size and weight of conventional hyperspectral spectrometer technologies (left). Note the significant difference in scale of the two images.

In our current project, we are developing a hyperspectral imaging system, shown schematically in Figure 1. Our technology (Figure 1b) uses a metasurface to precisely target very narrow spectral bands of interest, enabling a significant reduction in the size and number of optical components relative to current state-of-the-art imaging systems (Figure 1a), which in turn will enable the integration of our high-performance sensor onto weight-sensitive platforms (ie. satellites) far more readily than existing systems. Our initial goal is to detect and image trace gases in the Earth's atmosphere in the midwave infrared (MWIR), defined as 3-5 μm wavelength, while minimizing dependence on the Angle of Incidence (AoI) of light upon the sensor, up to an angle of 12° off-normal.

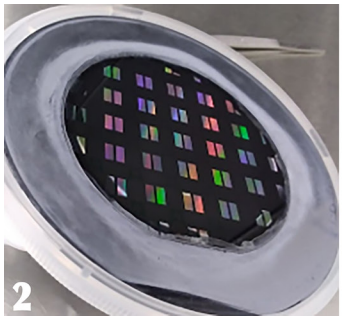

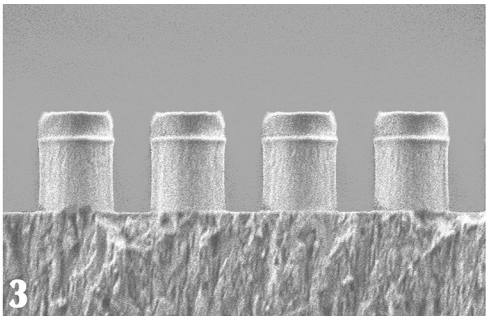

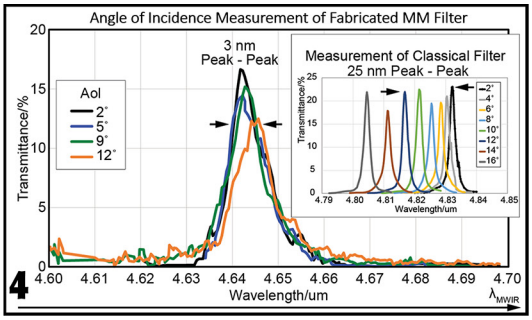

Figure 2: Wafer lithographically patterned with optical metastructures, using the ASML DUV stepper

Figure 3: SEM image (cross section) of etched pillars with near-vertical sidewalls. Imaged at ~ 15kX in the Ultra SEM, the grain structure of the etch stop layer is clearly visible.

Figure 4: Measured optical performance of fabricated metamaterial filter showing the angle of incidence independence up to a cone of 12° (f/2.4). (Inset) Same measurement performed on a classical Fabry-Pérot filter. Reproduced from reference 9.

Using the ASML DUV stepper, entire wafers can rapidly be lithographically patterned with highly uniform, large-area arrays of metastructures, as shown in Figure 2. In general, the optimal feature size and period of these metastructures depends primarily upon the desired wavelength of operation and the refractive indices of the constituent materials. In the MWIR, typical feature sizes are on the order of ~ 1 μm. Equally critical for minimizing optical losses in photonics applications, the relatively narrow spaces between features can be etched to form high-aspect-ratio structures with nearly vertical sidewalls, as shown in Figure 3.

Conclusions and Future Steps:

With strong, ongoing support from the National Aeronautics and Space Administration (NASA), we have successfully completed three generations of MWIR devices. As shown in Figure 4, they demonstrated the desired AoI insensitivity up to 12°. As we finish optimizing a few key process improvements in our fourth generation devices, we are beginning to integrate pixelated versions of our MWIR devices with commercially available ROIC's, for incorporation into a full camera system.

In addition, we are adapting our metasurface technology to other spectral ranges, from the visible to the microwave, by substituting appropriate materials, and scaling feature sizes as appropriate to the imaging wavelength. The extensive resources of the CNF are enabling us to rapidly develop our Metamaterial Spectrometer technology for a broad range of imaging and sensing applications.

References:

[1] Ebbesen, T.W., et al. "Extraordinary optical transmission through sub-wavelength hole arrays." Nature, (1998). 391(6668): p. 667-669.

[2] Crouse, D. "Numerical modeling and electromagnetic resonant modes in complex grating structures and optoelectronic device applications." Electron Devices, IEEE Transactions on 52.11 (2005): 2365-2373.

[3] Crouse, D., et al. "Polarization independent enhanced optical transmission in one-dimensional gratings and device applications." Optics Express 15.4 (2007): 1415-1427.

[4] Lansey, E., et al. "Light localization, photon sorting, and enhanced absorption in subwavelength cavity arrays." Optics Express 20.22 (2012): 24226-24236.

[5] Jung, Y.U., et al. "Dual-band photon sorting plasmonic MIM metamaterial sensor." Proc. SPIE 9070, Infrared Technology and Applications XL, 90702X (June 24, 2014); doi:10.1117/12.2050620.

[6] Crouse, D., et al. "A method for designing electromagnetic resonance enhanced silicon-on-insulator metal–semiconductor–metal photodetectors." Journal of Optics A: Pure and Applied Optics 8.2 (2006): 175.

[7] Mandel, I., et al. Theory and Design of A Novel Integrated Polarimetric Sensor Utilizing a Light Sorting Metamaterial Grating. Sensors Journal, IEEE, (2012): Vol. PP, 99

[8] Lepak, L., et al. "Handheld chem/biosensor using extreme conformational changes in designed binding proteins to enhance surface plasmon resonance (SPR)" Proc. SPIE 9862, Advanced Environmental, Chemical, and Biological Sensing Technologies XIII, 9862-7 (April 17, 2016); doi:10.1117/12.2222305.

[9] Bendoym, I., et al. "Low SWaP-C hyperspectral metamaterial spectrometer (MMS) for narrow-band, wide angle-of-incidence MWIR atmospheric sensing," Proc. SPIE 12091, Image Sensing Technologies: Materials, Devices, Systems, and Applications IX, 120910J (30 May 2022); https://doi.org/10.1117/12.2632794.

optiXphere Sensor Development

CNF Project Number: 3101-23
Principal Investigator & User: Tom Dunbar

Affiliation(s): tomPhyzx.LLC

Primary Source(s) of Research Funding: tomPhyzx.LLC, NYS Advanced Materials Grant (NYSTAR-AMT MEP)

Contact: tom@tomPhyzx.com, tom@uvcPhyzx.com

Research Group Website: tomPhyzx.com

Primary CNF Tools Used: CHA Evaporators, ABM Contact Aligner, Heidelberg DWL2000, YES Polyimide Oven

Abstract:

The optiXphere project aims to develop an omnidirectional UV-C detector. This report summarizes the progress made in substrate development, coating methods, and photolithographic techniques over the past year. Key advancements include refining the aluminum evaporation process, developing a wax resist etching technique, and constructing a projection lithographic system. These efforts have significantly improved the uniformity of photocurrent response across the substrate, moving closer to achieving a nearly flat detection curve.

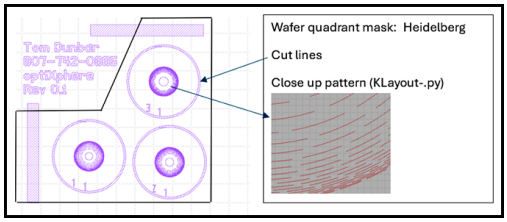

Figure 1: Quadrant mask design used for initial pattern transfer attempts.

Summary of Research, 2023-2024 Progress:

Substrate Development. Initial substrates were received from a Vermont Lampworker. A contract for substrate molding production was undertaken, resulting in near production-quality components. The refinement in the lampworker's process has ensured that the substrates are of high quality and suitable for subsequent experimental phases. The ability to produce substrates that meet the desired specifications has been a critical step in advancing the project.

Coating Methods. Various coating methods and CHA evaporations were evaluated, reducing UV-C photocurrent non-uniformity from four to two orders of magnitude. This significant improvement highlights the effectiveness of the refined coating techniques, paving the way for consistent and reliable substrate performance in future experiments. The evaluation of different methods has allowed for optimization of the coating process, ensuring that the substrates meet the necessary quality standards.

Nanoimprint Pattern Transfer Attempts. Initial attempts using SU-8 photoresist and Sylgard 185 molds for pattern transfer were abandoned due to mold press issues and limitations in feature size. The process aimed to create diffractive patterns, Figure 1, on the substrate but faced challenges in achieving the desired precision and resolution. Despite these challenges, valuable insights were gained, leading to the development of alternative approaches for pattern transfer.

New Approach 1, Projection Photolithography. Aluminum evaporation over the full substrate using the ODD-hour evaporator and a custom-built projection photolithographic stepper was pursued. A simplistic rotator system was developed as an accessory for the CHA Thermal evaporator to improve substrate coating uniformity.

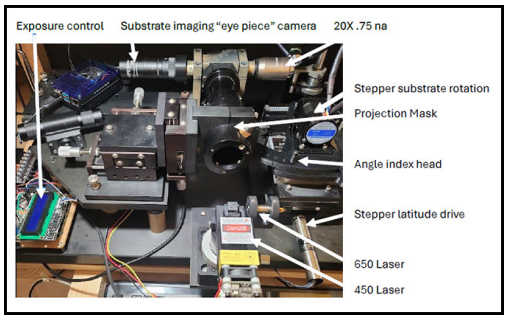

Figure 2: Custom-built projection photolithographic stepper system.

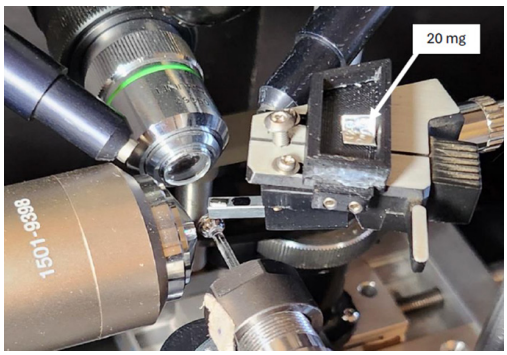

Figure 3: Custom-built wax scribing system.

This new approach addressed the limitations of previous methods, allowing for more precise control over the coating process and resulting in better substrate uniformity. The ability to achieve uniform coatings has been crucial in improving the overall performance of the substrates.

System Construction, Figure 2. A projection system with on-axis imaging was constructed to evaluate focus on spherical substrates. Exposures were made using a Young's double slit pattern, revealing resolution limitations. The system included a 650 nm dimmable diode laser for focusing and a 450 nm laser for exposure, controlled by an Arduino microcontroller. This setup enabled detailed examination of the substrate surface and the quality of the photolithographic process, providing critical insights for further refinements. The construction of this system has been a key development, allowing for precise control and evaluation of the photolithographic process. Resolution limitations using the current system components have shelved this approach for now.

New Approach 2, Wax Resist Etching. Inspired by Renaissance glassmaking techniques, wax-coated substrates were scribed and etched, creating thin horizontal features. Initial experiments using atomic force microscope probes were unsuccessful, leading to the planned use of microtome blades for more robust scribing. This wax resist technique, dubbed "Plow Lithography," involved detailed scribing of the wax layer followed by etching to expose the underlying aluminum, creating the desired patterns. The development of this technique should provide a reliable method for creating the necessary patterns on the substrates, Figure 3.

Funding and Collaboration:

Supplemental funding was secured through the NYS Advanced Materials Initiative Grant with MEP partnership with the Alliance for Manufacturing and Technology. Collaboration with Glassomer for substrate development is ongoing, with the first prototypes expected soon. The grant supplies in part CNF experiment expenses. These collaborations have provided essential resources and expertise, enabling significant progress and ensuring that the project stays on track. The funding and collaborative efforts have been instrumental in advancing the project and overcoming various challenges.

Experimental Results:

The first set of suitably coated substrates provided promising photocurrent results, showing a significant reduction in non-uniformity, Figure 4. The raw uncoated substrate had a four orders of magnitude non-uniformity, which was reduced to two orders with aluminum coating. This marked improvement validates the new coating and patterning techniques and demonstrates their potential for producing high-quality detectors. The experimental results have been encouraging, providing a strong foundation for further development.

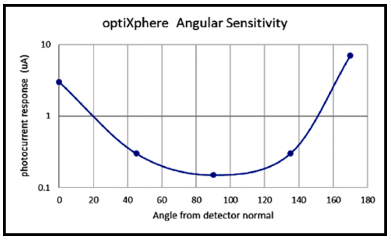

Figure 4: Photocurrent response versus latitude location on the substrate.

Process Challenges:

The initial pattern transfer approach faced challenges with mold pressing and achieving sub-micron feature sizes. The wax resist etching process also encountered difficulties, particularly with the surface roughness and speed limitations using atomic force microscope probes. These issues prompted the development of a more robust scribing technique using microtome blades. Addressing these challenges is crucial for achieving the desired precision and consistency in the substrate features, ensuring the final product meets the stringent requirements for UV-C detection. The challenges encountered have highlighted the need for continuous refinement and adaptation of the techniques used.

Conclusions and Future Steps:

The optiXphere project has made significant strides in substrate coating and patterning techniques. However, challenges remain in achieving the desired feature sizes and uniformity. Future efforts will focus on refining the wax resist etching process, developing stronger scribing tools, and exploring reflow transfer techniques for conformal 3D microprinting. Continued collaboration with CNF and external partners will be crucial in advancing the project towards a commercial-ready detector. Achieving a nearly flat photocurrent response across the substrate remains the ultimate goal, ensuring consistent and reliable detection of UV-C light, which is essential for practical applications in various fields. The future steps outlined will build on the progress made and address the remaining challenges to achieve the project's goals.

References:

[1] Zabow, G. (2022). Reflow Transfer for conformal 3-dimensional microprinting. NIST patent pending.

Dual-Band Metalenses for Imaging and Absolute Temperature Detection

CNF Project Number: 3105-23
Principal Investigator(s): Jason G. Valentine
User(s): Rahul Shah

Affiliation(s): Mechanical Engineering, Vanderbilt University

Primary Source(s) of Research Funding: Federal Grant

Contact: jason.g.valentine@vanderbilt.edu, rahul.shah.1@vanderbilt.edu

Primary CNF Tools Used: Gamma, ASML DUV Stepper, Heidelberg 2000, Oxford 81/82, Anatech Strip Resist, SEM

Abstract:

The project focuses on developing a novel dual-band metalens system, engineered for precise detection and identification of unknown aerial objects, with potential military applications. The design incorporates two metalenses that operate in distinct mid-infrared bands designed using a hyperbolic phase profile for diffraction-limited focusing enabling maximum angle resolution [1]. The metalenses are integrated with wavelength-selective filters for enhanced performance and compactness.

Summary of Research:

Trip 1: 2/4/24 – 2/10/24

- Orientation and training on the Gamma, ASML DUV Stepper, Heidelberg 2000, E beam deposition tool and in general chemistry.
- Generated mask for two lenses and patterned multiple wafers.
- The process aimed to deposit a hard mask and perform lift-off at The Vanderbilt Institute of Nanoscale Science and Engineering (VINSE). However, due to the large diameter of the lens (20 mm), lift-off proved challenging, resulting in incomplete liftoff and rendering the samples unusable for further processing and testing as seen in Figure 1.

Trip 2: 3/11/24 – 3/21/24

- Training on Oxford 81/82, Oxford Cobra, Anatech Resist Strip, and Scanning Electron Microscope (SEM).
- Employed a new strategy of depositing mask material (SiO2) on wafer before patterning to avoid having to lift-off of the hard mask.
- Generated mask for two samples and patterned multiple wafers.
- Post-processed the wafers to etch the anti-reflective coating (ARC), etch hard mask using a CHF_3/Ar recipe, and then ash-etch the rest of the resist and ARC, preparing the sample for Si etch.
- Attempted to Si etch using multiple recipes on the Oxford Cobra; however, a straight edge etch was not achieved as seen in Figure 2.
- Using a CHF_3/O_2 etch recipe for the hard mask, samples were Si etched at VINSE, achieving a vertical edge etch as seen in Fig. 3.
- Characterization revealed significant reduction in the size of the fabricated pillars compared to the designed ones due to diffraction effects during exposure and edge etching during mask and Si etch. The smallest design features were not patterned, leaving empty spaces on the wafer, as seen in Figure 2 and Figure 3.

Trip 3: 5/16/24 – 5/22/24

- To account for the discrepancy between fabricated pillar and designed pillar sizes, a bias was added to the design to compensate for the shrinkage during patterning and etching.
- Generated new masks incorporating the bias and patterned multiple wafers.
- Post-processed the samples, preparing them for Si etch at VINSE.
- After Si etch at VINSE, the lenses were characterized, and pillars covered entire lens surface as seen in Figure 4.

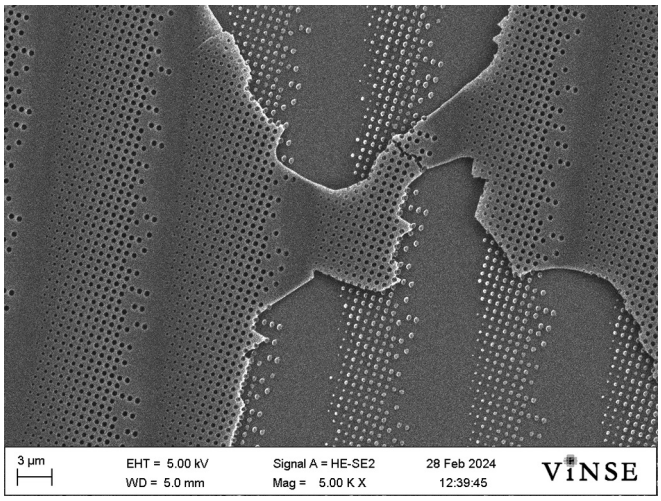

Figure 1: SEM images of the lens showing incomplete lift-off of the mask from the lens.

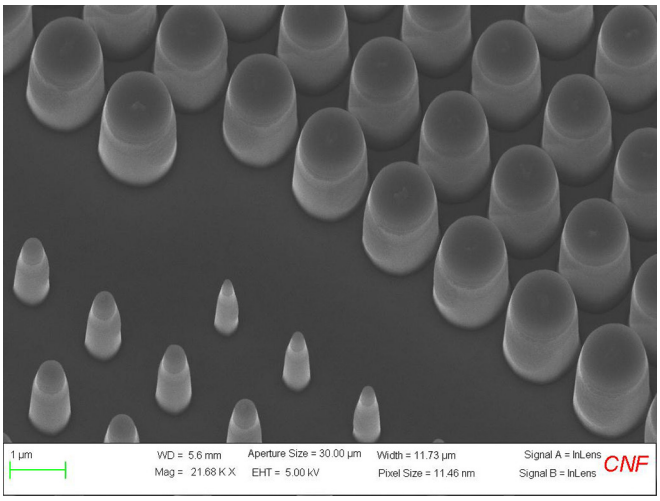

Figure 2: SEM image of the lens after Si etch at CNF showing pillars without perfectly vertical side walls. Rows of missing pillars visible.

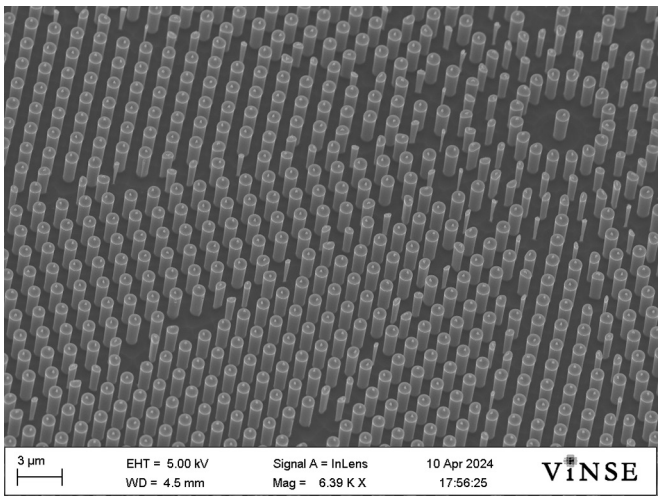

Figure 3: SEM image of the lens after Si etch at VINSE using a different mask etch recipe, showing improved side wall profile. Rows of missing pillars visible.

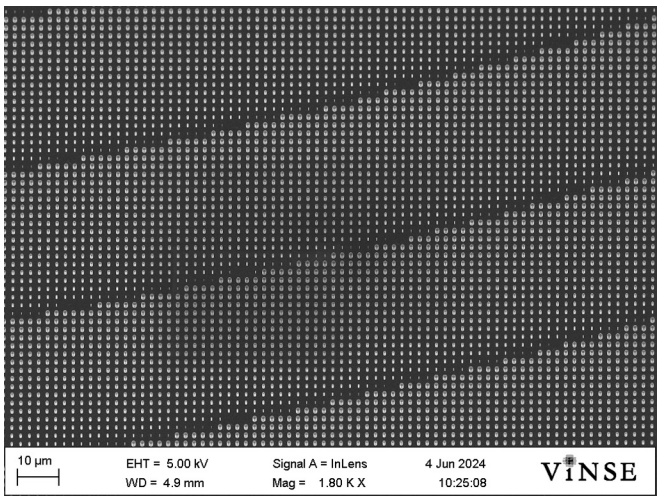

Figure 4: SEM image of the lens patterned after biasing, and after Si etch at VINSE with complete lens surface covered with pillars.

Conclusion and Future Steps:

The two lenses are designed to operate at a narrow band, and to ensure optimal performance, both lenses need to be equipped with a narrow band filter. We aim to design and fabricate a distributed Bragg reflector (DBR)-cavity-DBR based band pass filter on one side of the wafer and pattern and etch the lens on the other side of the wafer to achieve a seamless, compact design for our metalens. After fabrication and characterization, the lenses will undergo extensive testing to ensure they meet the necessary performance standards for the desired application.

References:

[1] Mohammadreza Khorasaninejad, et al., Metalenses at visible wavelengths: Diffraction limited focusing and subwavelength resolution imaging. Science352,1190-1194(2016). DOI:10.1126/science.aaf6644.

Diffractive Optical Element Manufacturing Feasibility

CNF Project Number: 3141-24
Principal Investigator(s): Chris Poulsen
User(s): Chris Poulsen, Alex Beam

Affiliation(s): Applied Image Inc.

Primary Source(s) of Research Funding: Applied Image Inc.

Contact: cpoulsen@appliedImage.com, abeam@appliedimage.com

Primary CNF Tools Used: GCA 5x g-line Stepper, Oxford 100 Plasma Etcher, YES Eco-Clean Asher, KLA P7 Profilometer

Abstract:

The purpose of this project is to investigate the feasibility of manufacturing a specific diffractive optical element (DOE) pattern using equipment available at both the Cornell NanoScale Facility (CNF) and at Applied Image, Inc. The pattern in question is a computer-generated hologram that acts as a high angle (170+ degrees) dot grid type beam splitter with 0.9 μm elements for use in an optical instrument.

Summary of Research:

Applied Image has set out to investigate whether it will be feasible to manufacture high quality DOEs using our current lithography equipment and resources like the Oxford 100 plasma etcher at CNF. Our test pattern that we are attempting to reproduce is a 49 x 49 0.900 μm binary pixel array with a pi phase shift, repeated over an entire 100 mm fused silica wafer.

Our first attempt to pattern our resist was using CNF. We used S1805 resist and a master made on our own lithography equipment with reticle markings for our GCA 5x G-Line stepper. Our stepper is nearly identical to the one at CNF, so we attempted to pattern our wafer using the stepper at CNF. The stepper at CNF is configured differently than ours and was unable to focus correctly on a clear substrate. The autofocus system on our stepper appears to be a completely different design, which allows it to focus properly.

One of our next tasks was to take the processes and training we received from CNF regarding resist spinning back to Applied Image. We completely redesigned the processes for our spin lab to mirror the best practices we learned during our training at CNF. Major changes were using pipettes for depositing resist, methods for depositing HMDS, increasing our accelerations and using a copper plate for cooling. Another important process related note, we have also launched a project to overhaul our safety procedures and documentation using CNFs safety manual as a gold standard.

After producing several wafers that were successfully patterned with AZ3312 resist, we took these back to CNF for processing in the Oxford 100 Plasma Etcher. We used two etch processes CHF_3/O_2 oxide etch (etch rate:150nm/min Selectivity 2.5:1), and C_4F_6/high He oxide etch (etch rate:225nm/min selectivity 4:1) [1]. An etch depth of 690 nm was targeted to create a pi phase shift in 632.7 nm He/Ne laser light.

An attempt was made to measure the etch depth of the pattern with the KLA P7 Profilometer. This did not turn out to be successful as the features were not quite big enough to get a good reading from the stylus. Most readings with the profilometer returned 125-275 nm etch depths. It was difficult to line up larger features (2 μm x 6 μm) as the viewing lens did not resolve these features very well. For better process control test patches with a larger cross-sectional area of at least 50 x 50 μm would need to be added to make better measurements on either a profilometer or an ellipsometer.

Despite the inability to measure or control the etch depth, reliance on the suggested etch rates seemed to be good enough to produce favorable results. Both etch methods produced an acceptable diffraction efficiency of around 90%. Although diffraction efficiency in terms of zero order energy to total beam energy were high, some undesirable artifacts were present in the form of lines between the desired dots in the resulting diffraction pattern. More investigation will be ongoing to attempt to resolve this issue.

Further work is being done to optimize the process including switching to ChemLab 5305 High-Resolution resist, that has so far shown superior resolution to Shipley S1805, AZ1505 and AZ3312 resists.

References:

[1] CNF Users. "Oxford 100 ICP Dielectric Etcher." Cornell NanoScale Science & Technology Facility. Etch Baseline Data. Accessed July 2, 2024.

OPTICS & OPTO-ELECTRONICS